

Guiding center orbit following calculation of edge particle and heat transport in stochastic magnetic field

C. C. Chang, Y. Nishimura ^{*}, and C. Z. Cheng

Institute of Space and Plasma Sciences, National Cheng Kung University, Tainan 70101, Taiwan

Received September 23, 2013

Key words Resonant magnetic perturbations, Magnetic islands, Orbit following calculation

Particle and heat transport in tokamak edge is investigated by guiding center orbit following calculation. The guiding center equation is solved for both electrons and ions in the presence of magnetic perturbation. It is suggested that the remnants of the magnetic islands play a role in characterizing the radial transport. The transport coefficient is estimated which also demonstrate local structure in the vicinity of magnetic islands.

Copyright line will be provided by the publisher

1 Introduction

Particle and heat transport in tokamak edge plays crucial roles in sustaining the plasma discharge. Externally imposed magnetic perturbation can induce magnetic stochasticity which can then prevent disruptive phenomena. [1] While magnetic field lines exhibit magnetic stochasticity in the presence of incommensurate magnetic perturbations, corresponding particle motions are also influenced by mirror force and perturbed electric fields.

The externally imposed Resonant Magnetic Perturbations (RMP) [1] degrades ion and electron particle transport while the electron heat transport does not change significantly (the electron mass transport component does not appear in the heat transport to the extent one expects from the density gradient [2]) and ion temperature rather rises. The latter feature is inconsistent with the Fick's law and Fourier's law in one dimensional diffusion model. These puzzling features are further confirmed in recent DIII-D experiments. [3, 4] A few possible ingredients are considered in this work to account for the inconsistency: (1) magnetic field lines are not completely stochastic [5] and the remnants of magnetic islands play a role, (2) trapped particles effects due to the equilibrium magnetic field inhomogeneity, (3) radial electric field and convective transport. [6] To investigate these latter effects, we employ a guiding center particle model.

Being different from self-generated tearing instabilities, [7] in the RMP experiments, magnetic perturbations are given by the external magnetic I-coils. From a computational point of view, the stochastic components of the magnetic field can be given time independent together with the equilibrium magnetic field. In this work, we would like to develop a numerical tool to investigate the tokamak edge transport. The guiding center equation is solved in the presence of magnetic perturbation. We would like to see the direct response of particles subject to the RMP. We then discuss density and temperature evolution by sampling the particles from the orbit calculation.

2 Computational model

The guiding center equation in a pseudo-toroidal coordinate [8] is given. Normalizing the length by the minor radius a , time by the inverse of the cyclotron frequency of electrons Ω_{ce} (or ions, Ω_{ci}), and the magnetic field strength at the magnetic axis B_0 , the guiding center equation components in the normalized units are given by

$$dr/dt = -\varepsilon\mu \sin(\theta) - v_{\parallel} \sum_m b_{rm} \sin(m\theta - n\zeta), \quad (1)$$

$$d\theta/dt = \varepsilon v_{\parallel}/q(r) - (\varepsilon\mu/r) \cos(\theta), \quad (2)$$

^{*} Corresponding author E-mail: nishimura@pssc.ncku.edu.tw

$$d\zeta/dt = \varepsilon v_{\parallel}, \quad (3)$$

$$dv_{\parallel}/dt = -[\varepsilon^2 \mu r/q(r)] \sin(\theta). \quad (4)$$

Here the normalized radial coordinate, the poloidal angle, and the toroidal angle are given by r , θ , and ζ respectively. The parallel velocity is given by v_{\parallel} and μ is the magnetic moment of the electrons and ions. In Eqs.(1)-(4), the normalized magnetic field strength is given by $B(r, \theta) = 1 - \varepsilon r \cos \theta$ where the inverse aspect ratio is given by ε . The safety factor is given by $q(r) = 1 + 3r^3$. As in the RMP experiments [1], we have taken a single toroidal mode number $n = 3$ and poloidal mode numbers $9 \leq m \leq 12$ in the computation. Each mode resonates at the mode rational surfaces $r_{m/n}$ where $q(r_{m/n}) = m/n$. To time advance Eqs.(1)-(4), a fourth order Runge-Kutta-Gill method is employed. The magnetic island width in the absence of the drift terms and the mirror force is given by $W_m = 2\sqrt{b_{rm}q(r_{m/n})^2/\sqrt{dq/dr}(r_{m/n})\varepsilon m}$. Here, W_m is independent of parallel velocity since (passing) particles freely stream along stochastic magnetic field lines.

3 Computational results

We investigate the evolution of the density and the temperature for the electrons and ions. Parameters used in the calculation are similar to the DIII-D tokamak, [1,3,4] major radius $R_0 = 3.0m$, minor radius $a = 1.0m$, toroidal magnetic field strength $B_0 = 2T$. We have taken the temperature at the pedestal top to be $T_i = T_e = 1keV$. The RMP amplitudes are given by $B_r/B_0 = 1.0 \times 10^{-3}$ (B_r is the radial component of magnetic perturbations) for all the $9 \leq m \leq 12$ ($n = 3$) modes which are about three times larger than the RMP experiments [1] (note that our safety factor profile is not as sharp as Ref. [1] and we took larger B_r values to have islands overlapped). Poincaré mapping of magnetic field lines are shown in Fig. 1(a) and Fig. 2(a). Figure 1(a) incorporates all the $9 \leq m \leq 12$ modes while Fig. 2(a) retains only the $m = 9$ mode to demonstrate the formation of a single magnetic island chain. Note that in the RMP experiments, the I-coil fields [1,3,4] are externally imposed ones and differ from self-generated tearing modes. [7] In Fig.1(a), one can observe significant amount of the island remnants. As a reference, the measured magnetic diffusion levels are $D_M = 1.48 \times 10^{-6}m$ at $r/a = 0.80$, $D_M = 3.06 \times 10^{-6}m$ at $r/a = 0.85$, and $D_M = 3.36 \times 10^{-6}m$ at $r/a = 0.90$ (Ref. [1] provides quasi-linear diffusion of $D^{ql} = 3.5 \times 10^{-6}m$).

Initial condition of the particles are given to satisfy the equilibrium density profile of $n(r) = n_0[1 - (r/a)^4]$ and the temperature profile of $T(r) = T_0[1 - (r/a)^4]$ for both the ions and electrons. Here n_0 and T_0 are the density and temperature at the magnetic axis. On each magnetic surface, the test particles are uniformly set in the poloidal angle on the $\zeta = 0$ plane. The velocity distribution is given by a bi-Maxwellian using a random number generator. [9] A total of 1,582,700 particles are used in the orbit following calculation.

When the particles reach $r/a = 1.0$ we remove them from the computation. We presume they are lost by reaching the divertor and then to the open-field-line scrape-off-layer regions. The divertor geometry is not included in this work, however. We only deal with closed magnetic field lines in this paper. Toward the core region, one finds Kolmogorov-Arnold-Moser (KAM) surface [near $r/a = 0.75$ in Fig.1(a)] which behaves as an inner reflection boundary for the particles. In the orbit following calculation, we set initial particles in the radial domain $0 \leq r/a \leq 1$, however. To estimate the density and the temperature evolution, we evolve the guiding center equation and after finite time assign particles into radially uniform bins. When the particles are in between mesh points, the particle density is assigned onto neighboring mesh points by a linear interpolation. Five hundred mesh points are taken within $0 \leq r/a \leq 1$. Unless there is a net radial transport (Coulomb collisional or stochasticity induced transport), the number of the particles conserves. For the temperature estimation, we take the second order velocity moments of the each particle and assign them into the radial bins.

Figure 1 (b) shows the electron density $n_e(r)$ evolution and Fig.1 (c) shows the electron temperature $T_e(r)$ evolution which are obtained from the guiding center calculation (in the presence of the RMP imposed stochastic magnetic field). The passing electrons are freely streaming along stochastic magnetic field lines. The trapped particles experience banana motion but they do not close on itself due to the perturbation (different from banana orbits in completely axisymmetric tokamaks). Since the magnetic field lines are stochastic, we observe effective radial diffusion. Figure 1 (b) and Fig.1 (c) show radial stepwise structure which reflects the remnants of magnetic islands. Since we have no source term but have a sink at $r/a = 1.0$, both the $n_e(r)$ and the $T_e(r)$ profiles

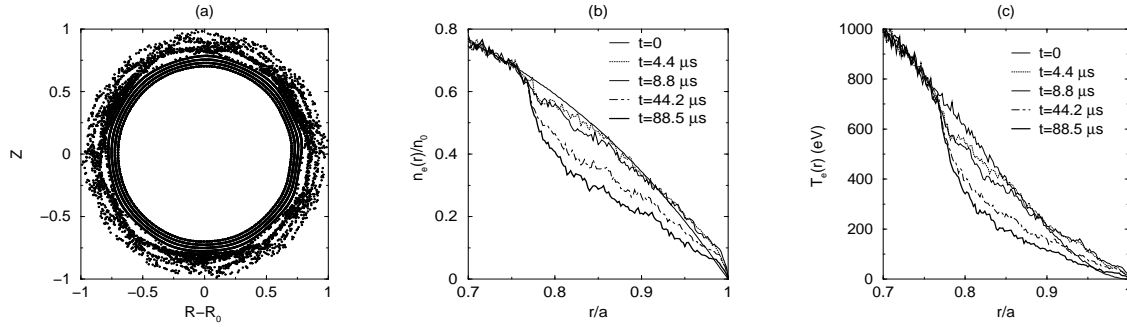


Fig. 1 (a) Poincaré plots of magnetic field lines in the presence of externally imposed magnetic field at the $\zeta = 0$ plane. Multiple poloidal modes ($9 \leq m \leq 12$) employed. Corresponds to guiding center Poincaré plots in the absence of mirror force and gradient-B drift. The radial and vertical coordinates are given by $R - R_0$ and Z respectively, where R is the major radius and R_0 is the major radius at the magnetic axis. (b) Electron density evolution, and (c) electron temperature evolution versus minor radius. Profiles are shown at $t = 0$, $t = 4.4(\mu s)$, $t = 8.8(\mu s)$, $t = 44.2(\mu s)$, and $t = 88.5(\mu s)$. Notice locally flattened structures due to the remnants of magnetic islands.

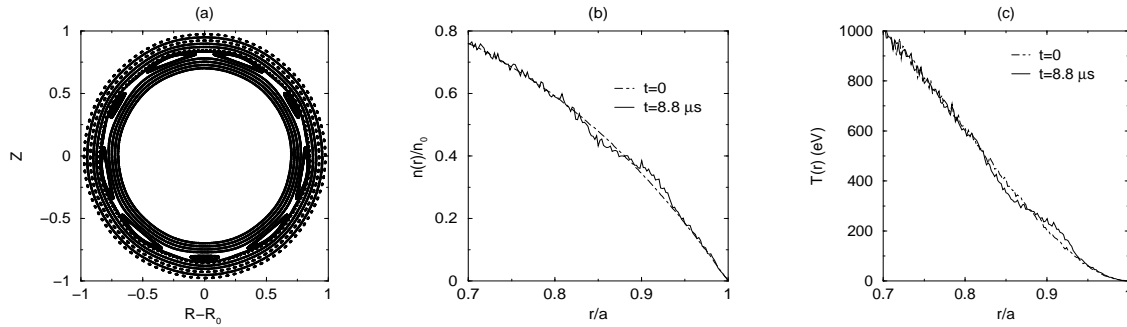


Fig. 2 (a) Poincaré plots of magnetic field lines in the presence of externally imposed magnetic field at the $\zeta = 0$ plane. A single poloidal mode ($m = 9$) is employed. (b) Electron density evolution, and (c) electron temperature evolution. Profiles are shown at $t = 0$ and $t = 8.8(\mu s)$. Observe the flattened structure in the vicinity of $0.8 \leq r/a \leq 0.85$. The flattened structure is due to the trapping of the passing particles by the $m = 9$, $n = 3$ magnetic island.

decay with time (corresponds to solving diffusion equation with a homogeneous Neumann boundary condition at $r/a \simeq 0.75$ and a Dirichlet boundary condition at $r/a = 1.0$).

To clarify the reflection of the magnetic island in the particle dynamics, a single $m = 9$ mode is incorporated in Fig.2. We observe flattening in the vicinity of the magnetic island. [10] The flattening is due to the trapping of the particles which rotate inside the magnetic island (due to the rotation, [11] the inboard side and the outboard side of the islands have approximately the same passing particle population). Note that what we see in Fig.1 (b)(c) and Fig.2 (b)(c) is merely a radial projection of the helically twisted three dimensional structure. On the other hand, note that the temperature evolution is due to the transport of particles themselves and is convective (conductive heat transport [12] is not incorporated in our model).

A series of computation in Fig.3 demonstrates evolution of ion density $n_i(r)$. Figure 4 is the evolution of the ion temperature $T_i(r)$, correspondingly. We have employed deuterium for the ion species. Figure 3(a) employs the same geometrical and field parameters with Fig.1. Note that for $T_i = 1000(keV)$ deuteriums, the banana width can be as large as a few percent of the minor radius. The time scale and the finite banana width are the major differences from the electron case. As in the electron case, KAM surface near $r/a \simeq 0.75$ behaves as a reflecting boundary. Both the ion density $n_i(r)$ and the ion temperature $T_i(r)$ decays with time. As for the electrons, a stepwise structure is found corresponding to the island remnants.

In Fig.3(b), we raise the amplitude of the magnetic perturbation. The magnetic perturbation is given by $B_r/B_0 = 4.0 \times 10^{-3}$ (increased by a factor of four from Fig.3(a), thus each magnetic island is twice larger). Note that the KAM surface is slightly shifted inward ($r/a \simeq 0.7$) compared to Fig.3(a). The stepwise structure

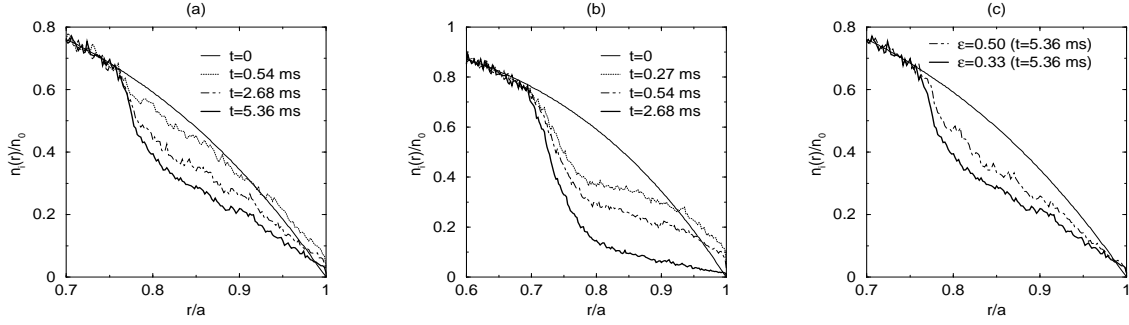


Fig. 3 Ion density evolution in the presence of $9 \leq m \leq 12$ ($n = 3$) modes. (a) The same parameters as in Fig.1 taken with profiles shown at $t = 0$, $t = 0.54(ms)$, $t = 2.68(ms)$, and $t = 5.36(ms)$, (b) the magnetic perturbation is given by $B_r/B_0 = 4.0 \times 10^{-3}$ with profiles shown at $t = 0$, $t = 0.27(ms)$, $t = 0.54(ms)$, and $t = 2.68(ms)$, and (c) the inverse aspect ratio of $\varepsilon = 0.5$ is taken and compared with the $\varepsilon = 0.33$ case at $t = 0.536(ms)$.

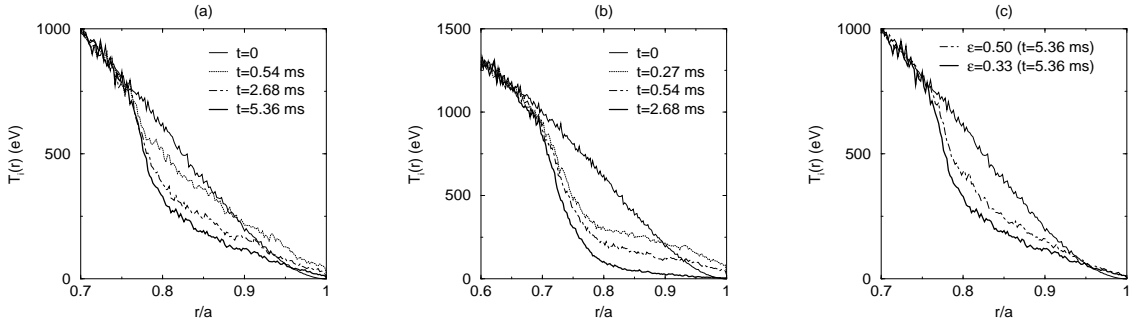


Fig. 4 Ion temperature evolution in the presence of $9 \leq m \leq 12$ ($n = 3$) modes. Corresponds to (a), (b), and (c) of Fig.3.

disappears accompanied by enhanced particle stochasticity and much rapid profile evolution. For Fig.3(a) and Fig.3(b), the inverse aspect ratio of $\varepsilon = 0.33$ is taken.

In Fig. 3(c), we vary the inverse aspect ratio ε and compare the time scale of the profile evolution with Fig. 3(a). The long dashed curve is for $\varepsilon = 0.5$ and the thick solid curve is for $\varepsilon = 0.33$. Both the curves are at $t = 5.36ms$ [see the thick solid curve in Fig.3(a) at $t = 5.36ms$]. The magnetic perturbation of $B_r/B_0 = 1.23 \times 10^{-3}$ is taken (to have the same magnetic island widths which depends not only on B_r but also on ε). Otherwise we take the same parameter as in Fig.3 (a). By the increase of the trapped particles' fraction, we find the transport level is reduced. By diagnosing single particle orbits, we found that the radial excursion of trapped particles is reduced. We conjecture the reduction of the transport level is due to the conservation of second adiabatic invariant for the trapped particles.

Local electron and ion diffusion coefficients D_e and D_i are calculated and shown in Fig.5. Figure 5(a) corresponds to Fig.1(b). Figure 5(b) corresponds to Fig.3(a). The transport coefficients are estimated by taking the second order moment of the test particles: $D_{e,i} = (1/N) \sum_{i=1}^N [(\Delta r_{e,i})^2 / 2\Delta t]$ where $\Delta r_{e,i}$ is the radial excursion of the particles (the electrons or the ions) measured with respect to the initial radial location. A sampling time is given by Δt . Here, N is the number of test particles which are set on a same radial location (and equidistantly in the poloidal angle). Note that D_e and D_i represent transport at the transient phase and not the ones at the steady state of a tokamak discharge. Relatively short sampling times are set for the electrons [$\Delta t = 4.4(\mu s)$] and for the ions [$\Delta t = 0.27(ms)$] because if the particles' spread is too large, the information of the local stochasticity is lost. Despite Fig.5 is generated by projecting the three dimensional motion onto the radial coordinate, we can observe non-monotonic structure. The degree of particle stochasticity varies in space. We again observe stepwise structure in the vicinity of $0.8 \leq r/a \leq 0.85$ for the ions (the D_e behavior within $0.82 \leq r/a \leq 0.85$ remains yet to be explained). The transport coefficients decrease near $r/a = 1.0$ due to the lower temperature of

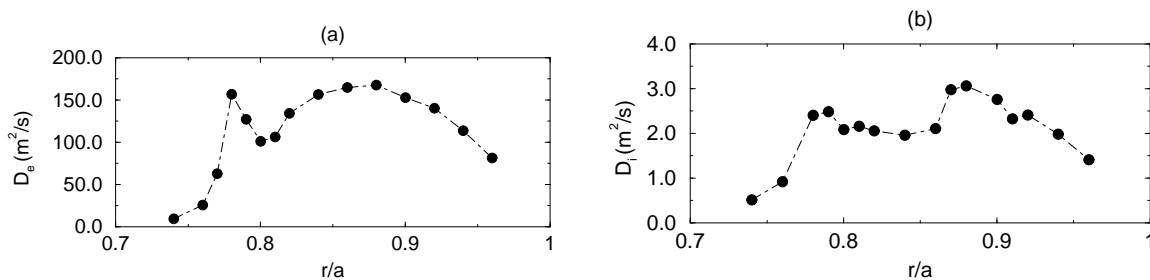


Fig. 5 (a) Electron diffusion coefficient D_e and (b) ion diffusion coefficient D_i as a function of radial location.

the test particles toward the edge. As a reminder, the temperature profile is given by $T(r) = T_0[1 - (r/a)^4]$ as an initial condition.

4 Summary and discussions

In this work, we have investigated tokamak edge particle and heat transport employing guiding center orbit following calculation in the presence of magnetic perturbation. From the orbit calculation, we have obtained the time evolution of radial density and temperature profile. Local diffusion coefficients are estimated by taking the second order moments of the test particles.

We have shown that the remnants of the magnetic islands can play a role in characterizing the radial transport. On the other hand, by raising the amplitude of the magnetic perturbation the stepwise structure disappeared accompanied by much rapid profile evolution. From the profile evolution and the diffusion coefficients, the remaining magnetic island regions can be regarded as a buffer for the radial transport (provides particles with relatively good confinement region). The island remnants effect can be related to the unresolved observation of the RMP experiments. [1] By increasing the trapped particle fraction, the transport level is reduced. The latter is related to the conservation of the second adiabatic invariants. [13] The projection of the particle dynamics onto the radial coordinate resembles diffusion process. [10] In actuality, what we see is the radial projection of the freely streaming electrons and ions along radially random walking stochastic magnetic field lines (with the correction of the mirror force [12] and the perpendicular drifts). The latter effects appear as parallel convection in the fluid model (the convective derivative originates from the streaming term in the Vlasov equation). We further plan to analyze the transport process by the fluid model. [14]

In this work, computational settings are not exactly that of tokamak RMP experiments. [1] For example, we did not have the divertor geometry. The safety factor, the density profile, and the temperature profile we used are given by a simplified model. Orbit calculation employing more realistic parameters (of the DIII-D tokamak, for example) will be our future work. One of the authors (YN) would like to thank discussions with Dr. R. A. Moyer, Dr. T. E. Evans, and Dr. L. E. Zakharov. This work is supported by National Science Council of Taiwan, NSC 100-2112-M-006-021-MY3. Computation of this work is performed on NVIDIA GPU cluster supported by National Cheng Kung University Top University Project and National Center for High-Performance Computing (NCHC) ALPS cluster of Taiwan.

References

- [1] T. E. Evans, R. A. Moyer, K. H. Burrell, *et al.*, *Nature Physics* **2**, 419 (2006).
- [2] R. A. Moyer (private communication, 2013).
- [3] T. W. Petrie, T. E. Evans, N. H. Brooks, *et al.*, *Nucl. Fusion* **51**, 073003 (2011).
- [4] O. Schmitz, T. E. Evans, M. E. Fenstermacher, *et al.*, *Nucl. Fusion* **52**, 043005 (2012).
- [5] A. B. Rechester and M. N. Rosenbluth, *Phys. Rev. Lett.* **40**, 38 (1978).
- [6] J. A. Wesson, B. Alper, A. W. Edwards, and R. D. Gill, *Phys. Rev. Lett.* **79**, 5018 (1997); A rapid convective inward transport of nickel is reported.
- [7] H. P. Furth, J. Killeen, and M. N. Rosenbluth, *Phys. Fluids* **6**, 459 (1963).
- [8] K. Miyamoto, *Plasma Physics for Nuclear Fusion*, 2nd ed. (MIT Press, Cambridge, 1989), P.41.

- [9] Y. Nishimura, *Comput. Phys. Commun.* **182**, 158 (2011); we initially focus on the collision-less particles.
- [10] Z. Chang and J. D. Callen, *Nucl. Fusion* **30**, 219 (1990).
- [11] D. R. Nicholson, *Introduction to Plasma Theory*, 2nd ed. (Kreiger, Malabar, 1992), P.92.
- [12] B. Chandran and S. Cowley, *Phys. Rev. Lett.* **80**, 3077 (1998).
- [13] A. J. Lichtenberg and M. A. Lieberman, *Regular and Chaotic Dynamics*, 2nd ed. (Springer, Berlin, 1992), P.21.
- [14] G. F. Chew, M. L. Goldberger, and F. E. Low, *Proc. Royal Soc. London A* **236**, 112 (1956).